# Tight-binding study of hcp Zn and Cd

X. W. Sha and D. A. Papaconstantopoulos
*School of Physics, Astronomy, and Computational Sciences, George Mason University, Fairfax, Virginia 22030, USA*

M. J. Mehl and N. Bernstein
*Center for Computational Materials Science, Naval Research Laboratory, Washington, DC 20375, USA*
(Received 1 September 2011; revised manuscript received 7 November 2011; published 28 November 2011)

We have developed tight-binding Hamiltonians for the hcp transition metals zinc and cadmium based on the Naval Research Laboratory tight-binding method. The Hamiltonians have a nonorthogonal basis and are derived by fitting to band structures and total energies of first-principles linearized augmented plane-wave calculations. We have applied this approach to compute the ground-state behavior, phase stability, band structures, densities of states, elastic moduli, and phonon frequencies for both Zn and Cd, and have found good agreement with available experimental and theoretical data in most cases. This approach also enables us to perform large-scale molecular dynamics simulations to calculate the vacancy formation energies, atomic mean-square displacements and coefficients of thermal expansion, at a small fractional cost of computational times compared with first-principles techniques.

DOI: 10.1103/PhysRevB.84.184109 PACS number(s): 71.15.Ap, 71.15.Nc, 71.20.−b, 71.15.Pd

## I. INTRODUCTION

The Naval Research Laboratory tight-binding (NRL-TB) method is based on the two-center Slater-Koster[1,2] formulation of tight binding with a nonorthogonal basis, taking advantage of the fact that the density functional theory[3,4] allows an arbitrary shift in the potential,[5,6] which makes it possible to fit the total energy without employing an empirical potential. The form of the NRL-TB parameters allows excellent transferability to different crystal structures and atomic configurations, and has been successfully applied to examine various structural, electronic, energetic, and dynamical properties of many transition and noble metals,[5–18] semimetals,[19] heavy metals,[20] semiconductors,[21–23] alloys,[24–27] carbon nanostructures,[28–30] and metal oxides,[31–33] etc. In particular, NRL-TB Hamiltonians have been previously developed for all the transition metals, except for column IIB. Here we applied the NRL-TB method to the hcp transition metals zinc and cadmium. Both Zn and Cd differ significantly from the typical transition metals that have a low-lying $s$ band and another five $d$ bands that progressively fill up so that the Fermi level ($E_f$) is either within the $d$ bands or just above for the noble metals. On the contrary, Zn and Cd have deep $d$ bands which fall between the first predominantly $s$-like band and a seventh band with $s$-$p$ character crossed by $E_f$. The situation is also different from some free-electron metals such as Al that have no occupied $d$ bands. In contrast to most hcp metals, Zn and Cd have unusually large axial ratios which are well above the ideal hcp ratio[34] and thus have some unique material properties such as the lowest melting points in transition metals aside from mercury. In Sec. II we detail the theoretical methods used to develop the NRL-TB Hamiltonians and perform tight-binding molecular dynamics simulations. In Sec. III we present the results and related discussions on various tight-binding derived properties obtained from both the static calculations and molecular dynamics simulations, and conclude with a brief summary in Sec. IV.

## II. THEORETICAL METHODS

In the two-center nonorthogonal NRL-TB scheme, the Slater-Koster terms include both the environment-dependent on-site parameters and the bond-length-dependent hopping parameters.[5,35] The on-site terms are assumed to be diagonal and have a polynomial form as a function of the atomic density. For a single element, the density of atom $i$ is defined as

$$\rho_i = \sum_j \exp(-\lambda^2 R_{ij}) F_C(R_{ij}), \tag{1}$$

where the sum is over all the neighboring atoms $j$ within a range of cutoff distance $R_c$ of atom $i$, $\lambda$ is a fitting parameter, and $F_C(R_{ij})$ is a smooth cut-off function. The angular-momentum-dependent on-site terms are defined by

$$h_\ell = a_\ell + b_\ell \rho^{2/3} + c_\ell \rho^{4/3} + d_\ell \rho^2, \tag{2}$$

where $\ell$ represents the $s$, $p$, and $d$ orbitals, and $a_\ell$, $b_\ell$, $c_\ell$, and $d_\ell$ are our fitting coefficients.

We construct the two-center *spd* Slater-Koster (SK) hopping integrals from the ten independent SK parameters, which are assumed to all have polynomial times exponential forms in terms of neighbor distance

$$P_\gamma(R) = \sum_j (e_\gamma + f_\gamma R + g_\gamma R^2) \exp\left[-q_\gamma^2 R\right] F_c(R), \tag{3}$$

where $\gamma$ indicates the type of interactions, including $ss\sigma$, $pp\sigma$, $sp\sigma$, $dd\sigma$, $sd\sigma$, $pd\sigma$, $pp\pi$, $dd\pi$, $pd\pi$, and $dd\delta$. $R$ is the distance between the atoms, and $e_\gamma$, $f_\gamma$, $g_\gamma$, and $q_\gamma$ are our fitting coefficients. We define the Slater-Koster overlap functions in a nonorthogonal calculation to have the same form as the hopping parameters. Overall, there are in total 93 fitting coefficients for a single element in the on-site, hopping, and overlap terms in the NRL-TB Hamiltonians with $s$, $p$, and $d$ orbitals, and the values of these fitting coefficients for Zn and Cd are listed in Table I.

 

TABLE I. Tight-binding coefficients for Zn and Cd, generated by fitting to the first-principles LAPW total energies and band structures of bcc, fcc, hcp, and simple cubic structures.

| | | | | |
|---|---|---|---|---|
| | | Zn | | |
| | | On-site parameters ($\lambda = 1.469991$ a.u.$^{-1/2}$) | | |
| | | $\rho_i = \sum_j \exp(-\lambda^2 R_{ij}) F_C(R_{ij})$ | | |
| | | $h_\ell = a_\ell + b_\ell \rho^{2/3} + c_\ell \rho^{4/3} + d_\ell \rho^2$ | | |
| $\ell$ | $a_\ell$ | $b_\ell$ | $c_\ell$ | $d_\ell$ |
| $s$ | 0.22328 | 33.46771 | −5376.929237 | 530223.036806 |
| $p$ | 0.697637 | 10.633128 | −4414.114916 | 858194.489409 |
| $d$ | −0.032554 | −1.145394 | 339.451793 | −73547.97693 |
| | | Hopping terms | | |
| | | $P_y(R) = \sum_j (e_y + f_y R + g_y R^2) \exp\left[-q_y^2 R\right] F_c(R)$ | | |
| $\gamma$ | $e_\gamma$ | $f_\gamma$ | $g_\gamma$ | $q_\gamma$ |
| $ss\sigma$ | 2.630211 | −1.072291 | 0.049662 | 0.800106 |
| $sp\sigma$ | 1.702888 | 0.371463 | 0.119067 | 1.022335 |
| $pp\sigma$ | −0.138547 | 0.077519 | 0.001158 | 0.660035 |
| $pp\pi$ | −3.547105 | 0.662968 | 0.02738 | 0.788917 |
| $sd\sigma$ | −0.088475 | −0.139397 | 0.00354 | 0.834245 |
| $pd\sigma$ | −0.480234 | 0.082434 | 0.004016 | 0.839235 |
| $pd\pi$ | 9.892114 | 0.247499 | −0.585076 | 0.981195 |
| $dd\sigma$ | 1.573334 | 0.054652 | −0.204651 | 1.042584 |
| $dd\pi$ | 5.528614 | −0.835957 | 0.046933 | 1.037825 |
| $dd\delta$ | −160.313912 | −9.176101 | 7.146619 | 1.358961 |
| | | Overlap terms | | |
| | | $S_y(R) = \sum_j (\delta_y + t_y R + r_y R^2) \exp\left[-u_y^2 R\right] F_c(R)$ | | |
| $\gamma$ | $\delta_\gamma$ | $t_\gamma$ | $r_\gamma$ | $u_\gamma$ |
| $ss\sigma$ | −40.426164 | 13.824170 | 0.064994 | 1.063141 |
| $sp\sigma$ | 8.349221 | −3.406862 | −0.124509 | 0.895341 |
| $pp\sigma$ | −0.758428 | −0.047789 | 0.002815 | 0.549763 |
| $pp\pi$ | 1.905233 | −0.050823 | −0.008351 | 0.666625 |
| $sd\sigma$ | 5.482247 | −1.123358 | −0.072468 | 0.848286 |
| $pd\sigma$ | 1.096869 | 0.443588 | −0.23008 | 0.860846 |
| $pd\pi$ | 317.522047 | −47.939737 | −6.193006 | 1.188616 |
| $dd\sigma$ | 2179.46986 | 466.04847 | −186.821306 | 1.442683 |
| $dd\pi$ | −2.729519 | 0.11063 | −0.093612 | 1.041364 |
| $dd\delta$ | 20.891994 | 0.38954 | −0.571871 | 1.00681 |
| | | Cd | | |
| | | On-site parameters ($\lambda = 1.605663$ a.u.$^{-1/2}$) | | |
| | | $\rho_i = \sum_j \exp(-\lambda^2 R_{ij}) F_C(R_{ij})$ | | |
| | | $h_\ell = a_\ell + b_\ell \rho^{2/3} + c_\ell \rho^{4/3} + d_\ell \rho^2$ | | |
| $\ell$ | $a_\ell$ | $b_\ell$ | $c_\ell$ | $d_\ell$ |
| $s$ | 0.363794 | 86.10881 | −76791.192088 | 108436393.485 |
| $p$ | 0.867613 | −127.036573 | 133590.464111 | 124813010.82 |
| $d$ | −0.06385 | 15.238177 | −20740.893262 | −2843236.2717 |
| | | Hopping terms | | |
| | | $P_y(R) = \sum_j (e_y + f_y R + g_y R^2) \exp\left[-q_y^2 R\right] F_C(R)$ | | |
| $\gamma$ | $e_\gamma$ | $f_\gamma$ | $g_\gamma$ | $q_\gamma$ |
| $ss\sigma$ | 5.724943 | −6.601102 | 0.015762 | 1.061474 |
| $sp\sigma$ | 0.245014 | −0.02487 | 0.000418 | 0.542236 |
| $pp\sigma$ | −31.355628 | 5.972695 | −0.038353 | 0.894364 |
| $pp\pi$ | 18.204678 | −0.142384 | −0.550664 | 1.01025 |
| $sd\sigma$ | −380.682071 | 88.930014 | −0.168741 | 1.212736 |
| $pd\sigma$ | 15.707529 | −3.273015 | 0.003657 | 0.890509 |
| $pd\pi$ | 2.011892 | 0.250708 | 0.027848 | 1.073848 |
| $dd\sigma$ | 58.263161 | −19.937689 | 0.347991 | 1.163757 |
| $dd\pi$ | 11.827992 | −1.5099 | 0.017756 | 1.013595 |
| $dd\delta$ | −4.736575 | 0.623097 | −0.001169 | 1.073331 |

TABLE I. *(Continued.)*

| $\gamma$ | $e_\gamma$ | $f_\gamma$ | $g_\gamma$ | $q_\gamma$ |
|---|---|---|---|---|
| | | Overlap terms | | |
| | | $S_y(R) = \sum_j (\delta_y + t_y R + r_y R^2) \exp[-u_y^2 R] F_C R$ | | |
| $\gamma$ | $\delta_\gamma$ | $t_\gamma$ | $r_\gamma$ | $u_\gamma$ |
| $ss\sigma$ | −0.392718 | 0.470493 | −0.033283 | 0.667106 |
| $sp\sigma$ | 59.630549 | −15.443898 | −0.204783 | 0.973806 |
| $pp\sigma$ | 6.28926 | −3.547458 | −0.134306 | 0.90149 |
| $pp\pi$ | 4.911012 | −0.602315 | 0.006926 | 0.754477 |
| $sd\sigma$ | 11.256193 | −0.07029 | −0.410407 | 1.030123 |
| $pd\sigma$ | 133.598176 | −11.940802 | −3.109452 | 1.097928 |
| $pd\pi$ | −33.085745 | 3.64351 | 1.411897 | 1.047261 |
| $dd\sigma$ | 4.848817 | 0.438177 | −0.121407 | 1.031423 |
| $dd\pi$ | −7.338715 | −0.233211 | 0.021357 | 1.002701 |
| $dd\delta$ | −26.229872 | 2.851133 | 0.782012 | 1.096638 |

For both Zn and Cd, we used the full-potential linearized augmented plane-wave (LAPW) total energy calculations[36,37] within the local density approximation (LDA)[4] to generate total energies and band structures for bcc, fcc, hcp, and simple cubic crystal structures with varying atomic volumes, and, in the case of the hcp structure, we fitted only selected total energy values and not a full range of values and $c/a$ ratios. The total energy is usually weighed at around 200–300 times over a single band energy. We are able to obtain fitting rms error of less than 5 mRy and 0.2 mRy for the energy bands and total energy, respectively.

We calculate the finite-temperature dynamical properties from tight-binding molecular dynamics simulations, which are performed in the microcanonical ensemble by integrating the equations of motion using Verlet's algorithm[38] and a time step of 2 fs. The forces on each atom are calculated from the eigenvectors of the TB Hamiltonian of the system using the Hellmann-Feynman theorem.[39] The supercells used in our molecular dynamics simulations contain 288 atoms, and we typically are able to approach equilibrium in the tight-binding molecular dynamics simulations within 2000 time steps (4 ps).

## III. RESULTS AND DISCUSSION

### A. Equilibrium structure and phase stability

The NRL-TB method's combination of computational efficiency and transferability to different crystal structures and atomic configurations enable us to examine low-symmetry crystal structures and defect structures, in addition to the high-symmetry bcc, fcc, hcp, and simple cubic phases used in the Hamiltonian fitting. In Table II, we list the calculated tight-binding total energies of Zn in 26 different crystal structures. Among all the structures examined, we find that the hcp structure is lowest in energy, consistent with experiment.[34] In Fig. 1(a) we show the volume dependence of the tight-binding total energies for fcc, bcc, simple cubic, hcp, and diamond structures. The tight-binding calculations successfully reproduce the first-principles LAPW data of the fcc, bcc, and simple cubic structures that are used in the development of the tight-binding Hamiltonians. For the hcp structure, we minimize the tight-binding total energies as a function of the $c/a$ ratio at each given volume, thus the tight-binding results are not directly comparable with the LAPW energies used in the tight-binding fitting due to the different $c/a$ ratios. The equilibrium volume for hcp Zn is somewhat underestimated in tight-binding (91.23 Bohr$^3$/atom), in comparison to the experiment at 102.56 Bohr$^3$/atom.[34] This discrepancy is mainly due to the use of the LDA in our input database, which usually underestimates the equilibrium volume of the $3d$ transition metals.[40] In contrast, previous first-principles calculations using generalized-gradient approximation (GGA) predict an equilibrium volume of 97.32 Bohr$^3$/atom,[41] in closer agreement with experiment. The tight-binding calculated $c/a$ ratio at the equilibrium ($c/a = 1.828$) is in good agreement with experiment ($c/a = 1.856$), similar to previous first-principles calculations.[41] Our tight-binding calculations find no significant anomaly in the $c/a$ ratio for hcp Zn under compression, consistent with hydrostatic high-pressure powder x-ray diffraction experiments[42] and first-principles calculations.[43]

The tight-binding predicted equilibrium properties of Cd are quite similar to those of Zn. The hcp structure also has the lowest energy among the 26 different crystal structures examined, as shown in Table III and Fig. 1(b). The tight-binding calculations underestimate the hcp equilibrium volume by ∼6.5%, in comparison with the experimental value of 145.63 Bohr$^3$/atom at ambient conditions, again due to the fitting of the Hamiltonians to LAPW calculations using the LDA approximation. The tight-binding calculations predict a $c/a$ ratio of 1.883 in close agreement with the equilibrium experimental value of 1.885, similar to the Zn results.

The fact that the LDA results, to which our TB fit was based, are in better agreement with experiment for Cd than Zn is consistent with previous findings. Indeed, the LDA results for the $4d$ metals better agree with the experiment than those for the $3d$ metals.[44]

### B. Electronic structure

At the ambient experimental equilibrium volume, the tight-binding calculated band structure and electronic density of states are in excellent agreement with first-principles LAPW results for both hcp Zn and Cd, as shown in Figs. 2 and 3.

TABLE II. The calculated tight-binding total energies of Zn in 26 different crystal structures. Tight-binding calculations correctly predict that hcp is the equilibrium structure, and its energy $E_0$ is the lowest among all the structures examined.

| Structure | Name | No. of atoms | $V$ (Bohr$^3$/atom) | $E-E_0$ (Ry/atom) |
|---|---|---|---|---|
| $A3$ | hcp | 2 | 91.23 | 0.00000 |
| $C19$ | $\alpha$-Sm | 3 | 91.75 | 0.00063 |
| $A3'$ | dhcp | 4 | 91.62 | 0.00079 |
| $A13$ | $\beta$-Mn | 20 | 93.97 | 0.00093 |
| $A_a$ | $\alpha$-Pa ($c/a = 0.77$) | 1 | 93.47 | 0.00129 |
| $A10$ | $\alpha$-Hg (51.5°) | 1 | 93.77 | 0.00246 |
| $A1$ | fcc | 1 | 90.45 | 0.00247 |
| $A12$ | $\alpha$-Mn | 29 | 92.60 | 0.00418 |
| $A_b$ | $\beta$-U | 30 | 91.46 | 0.00458 |
| $A7$ | $\alpha$-As | 2 | 98.39 | 0.00481 |
| $A15$ | $A15$ | 8 | 91.70 | 0.00539 |
| $A11$ | $\alpha$-Ga | 4 | 99.14 | 0.00550 |
| $A16$ | $\alpha$-S | 32 | 97.89 | 0.00745 |
| $A_f$ | Simple hexagonal | 1 | 101.96 | 0.00760 |
| $A8$ | $\gamma$-Se | 3 | 101.99 | 0.00769 |
| $A2$ | bcc | 1 | 91.90 | 0.00848 |
| $C32$ | $\omega$ | 3 | 93.34 | 0.00913 |
| bct5 | bct5 | 2 | 99.34 | 0.00968 |
| $A5$ | $\beta$-Sn | 2 | 104.43 | 0.01705 |
| $A_h$ | Simple cubic | 1 | 108.63 | 0.02181 |
| $hR12$ | $\alpha$-B | 12 | 122.10 | 0.02199 |
| $d2h$ | 2H diamond | 4 | 123.53 | 0.02990 |
| $A9$ | Graphite | 4 | 119.08 | 0.03511 |
| $A4$ | Diamond | 2 | 140.29 | 0.04553 |
| $E2_1$ | Perovskite | 5 | 128.76 | 0.05067 |
| $D0_9$ | $ReO_3$ | 4 | 173.36 | 0.06615 |

TABLE III. Same as Table II, but for Cd.

| Structure | Name | No. of atoms | $V$ (Bohr$^3$/atom) | $E-E_0$ (Ry/atom) |
|---|---|---|---|---|
| $A3$ | hcp | 2 | 136.23 | 0.00000 |
| $C19$ | $\alpha$-Sm | 3 | 136.74 | 0.00059 |
| $A3'$ | dhcp | 4 | 136.78 | 0.00080 |
| $A_a$ | $\alpha$-Pa ($c/a = 0.76$) | 1 | 139.19 | 0.00133 |
| $A10$ | $\alpha$-Hg (53.0°) | 1 | 137.69 | 0.00202 |
| $A1$ | fcc | 1 | 136.33 | 0.00323 |
| $A15$ | $A15$ | 8 | 138.05 | 0.00342 |
| $A13$ | $\beta$-Mn | 20 | 141.25 | 0.00379 |
| $A_b$ | $\beta$-U | 30 | 137.76 | 0.00423 |
| $A12$ | $\alpha$-Mn | 29 | 139.59 | 0.00518 |
| $A7$ | $\alpha$-As | 2 | 143.71 | 0.00711 |
| $A11$ | $\alpha$-Ga | 4 | 145.29 | 0.00756 |
| $A2$ | bcc | 1 | 137.99 | 0.00837 |
| bct5 | bct5 | 2 | 148.61 | 0.00840 |
| $A16$ | $\alpha$-S | 32 | 146.31 | 0.00849 |
| $C32$ | $\omega$ | 3 | 141.34 | 0.00869 |
| $A8$ | $\gamma$-Se | 3 | 149.32 | 0.01157 |
| $A_f$ | Simple hexagonal | 1 | 149.38 | 0.01160 |
| $A5$ | $\beta$-Sn | 2 | 151.81 | 0.01399 |
| $hR12$ | $\alpha$-B | 12 | 158.72 | 0.01408 |
| $A_h$ | Simple cubic | 1 | 157.49 | 0.01591 |
| $d2h$ | 2H diamond | 4 | 190.37 | 0.02893 |
| $A9$ | Graphite | 4 | 177.19 | 0.03081 |
| $A4$ | Diamond | 2 | 209.54 | 0.04040 |
| $E2_1$ | Perovskite | 5 | 187.21 | 0.05024 |
| $D0_9$ | $ReO_3$ | 4 | 298.49 | 0.06042 |

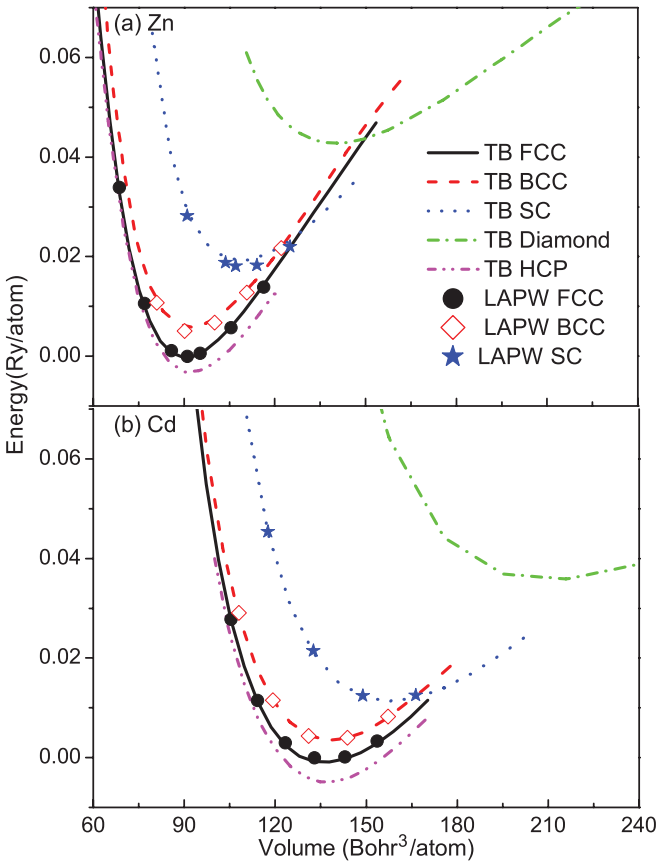


FIG. 1. (Color online) The tight-binding total energies (lines) of fcc, bcc, hcp, simple cubic, and diamond structures of Zn (a) and Cd (b) as functions of atomic volume, in comparison to the first-principles LAPW results (symbols) of fcc, bcc, and simple cubic structures used in the development of tight-binding Hamiltonians. The tight-binding hcp results here are not directly comparable to the LAPW values used in the fitting due to different *c*/*a* ratios.

For hcp Zn, the 3*d* bands are centered at ∼0.58 Ry below the Fermi level and mostly confined within a narrow range of ∼0.15 Ry. The 4*d* bands are located deeper in hcp Cd, at ∼0.66 Ry below the Fermi level with a narrow distribution of ∼0.15 Ry. For both hcp Zn and Cd, most bands around the Fermi level have mixed *s* and *p* character. Since the *d* bands are occupied and located far below the Fermi level, Zn and Cd should be viewed more like free-electron metals such as Mg, instead of as a typical transition metal, where *d* bands are generally close to the Fermi surface and play an important role in bonding.

The tight-binding calculated Fermi surfaces of hcp Zn at the ambient experimental equilibrium volume are in close agreement with first-principles LAPW results, as shown in Fig. 4. There are three major bands shown in the Fermi surfaces: one forming pockets around the upper and lower parts of each corner (the *H* point in the Brillouin zone) (green/yellow); the second (purple/blue) filling the entire corner (along the *K*-*H* line) and possibly connecting the corners (it is hard to be certain even using 11 000 *k* points); and the third, in light blue, filling the zone center. One noticeable difference between the tight-binding and LAPW surfaces can be found in the purple necks. In tight binding the neighboring necks tend to connect to each other, while in LAPW there are no connections. Such differences can be also seen in the band structure, where the tight-binding band goes just above the Fermi level and the LAPW band goes just below it in the Σ direction. For hcp Cd, the tight-binding and LAPW-calculated Fermi surfaces show better agreement, as shown in Fig. 5. There is no observable trend to connect the purple necks, and both tight-binding and LAPW predict the band energy below the Fermi level in the Σ direction.

### C. Elastic moduli

To calculate the elastic moduli, we impose volume-conserving external strains on the structure, relax any internal parameters to obtain the energy as a function of the strain, and numerically calculate the second derivative of the energy-strain curves.[45] As shown in Table IV, in hcp Zn our tight-binding calculations significantly underestimate the bulk modulus and some of the elastic moduli ($C_{13}$, $C_{33}$, and $C_{44}$), all by over 20 GPa, in comparison to the experiment.[46] The significant underestimation of $C_{13}$ and $C_{33}$ has been previously reported in density-functional theory calculations using both GGA and hybrid functionals for Zn.[47] The calculated bulk and elastic moduli of hcp Cd show much better agreement with the experiment; all agree within 8 GPa.[46]

### D. Phonon dispersion

Using the frozen phonon approximation,[48] we calculate the phonon dispersion curves along several high-symmetry directions in the Brillouin zone for both hcp Zn and Cd, as shown in Fig. 6. The phonon spectra were calculated using supercells generated by the PHON code[49] and Stokes's FROZSL code,[50] the calculations agreeing well with each other. Since these calculations are performed at the equilibrium volume and *c*/*a* ratio predicted by the tight-binding Hamiltonians and the tight-binding equilibrium volume is significantly smaller than the experimental value, it is not surprising to see that the tight-binding calculated phonon frequencies for hcp Zn and Cd are mostly 10%–20% higher than the inelastic neutron-scattering measurements.[51] Phonon frequencies generally increase significantly with volume compression (increase of the pressure) in transition metals, as shown in many previous experimental and first-principles calculations.[45,52–54]

### E. Atomic mean-square displacements

Atomic mean-square displacement (MSD) is an important materials parameter to describe the lattice vibrational properties at finite temperatures.[38] We calculate the MSDs based on the time-dependent atomic coordinates obtained through tight-binding molecular dynamics simulations at several selected temperatures.[38] The calculated MSDs for both hcp Zn and Cd show a linear increase with the increase of temperature, as shown in Fig. 7. Cd has a larger atomic MSD than Zn at all the temperatures we examined. We only report MSDs for Zn and Cd up to 500 K due to the low melting points of Zn (693 K) and Cd (594 K), and the fact that our tight-binding molecular dynamics simulations break when the temperature approaches the melting point. Our high-temperature tight-binding molecular dynamics simulations break at 750 K

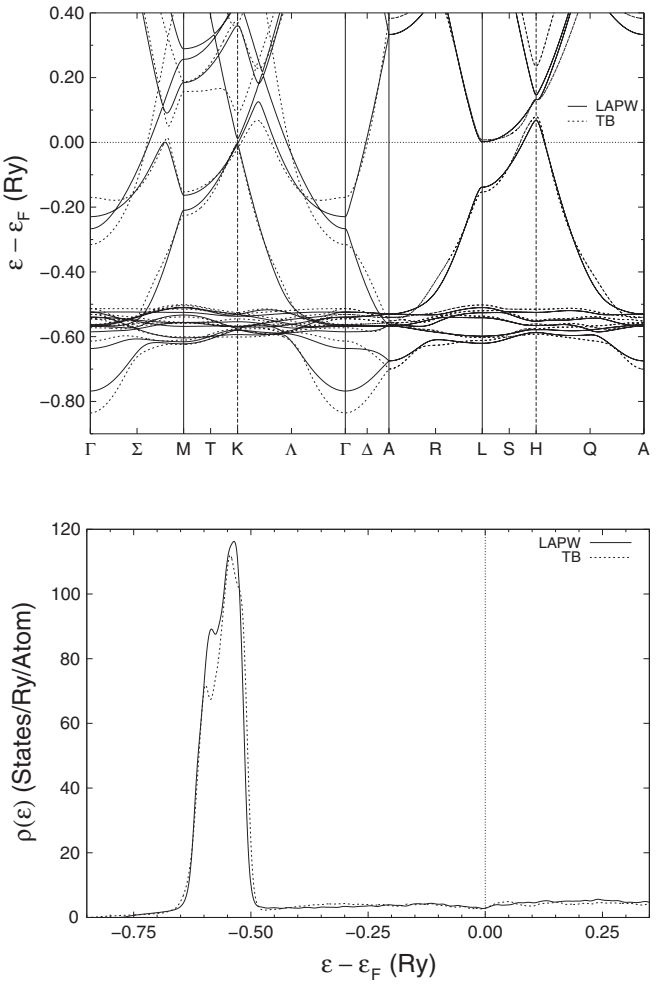


FIG. 2. The tight-binding band structure and electronic density of states of hcp Zn at the ambient experimental equilibrium volume agree well with first-principles LAPW results.

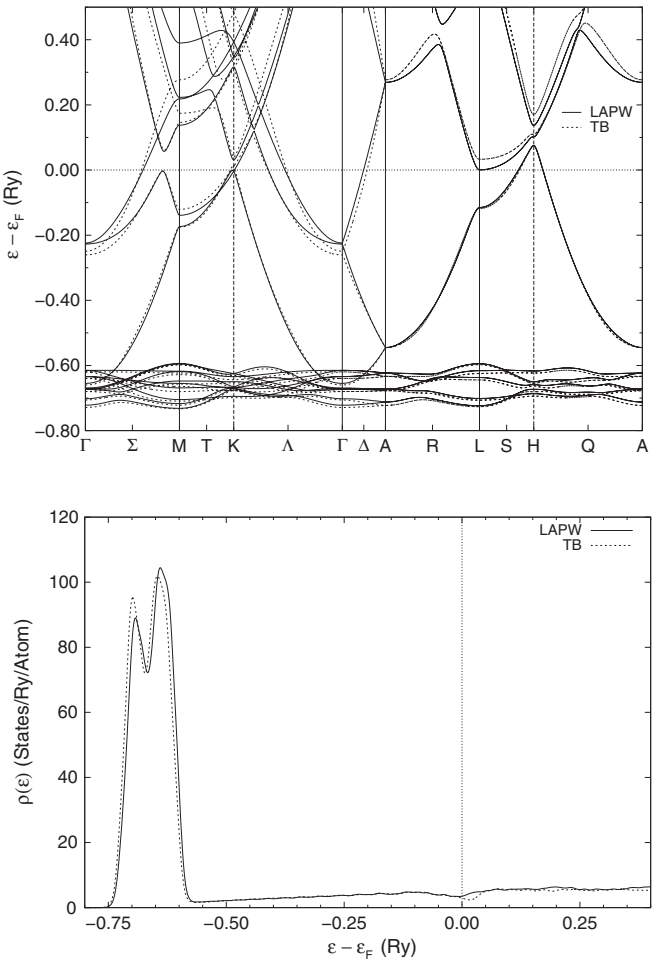


FIG. 3. Same as Fig. 2, but for hcp Cd.

for Zn and 525 K for Cd, which are both close to the experimental melting points. The calculated MSD values of Cd agree well with the experimental data derived from the Debye-Waller factor measurements,[55,56] especially at around the ambient temperature. The increasing differences between the calculated and experimental values at higher temperatures are partially due to the fact that we perform all the molecular dynamics simulations at constant volume. The tight-binding calculations underestimated the MSD values of Zn, partially due to the underestimation of ambient equilibrium volume.

### F. Coefficient of thermal expansion

The thermal expansion coefficient is a thermodynamic parameter that can also be obtained from our volume-conserving

TABLE IV. The tight-binding calculated bulk and elastic moduli for hcp Zn and Cd at the ambient experimental equilibrium volume are in reasonable agreement with experimental measurements (Ref. 46).

| | Elastic moduli (GPa) | | | |
|---|---|---|---|---|
| | hcp Zn | | hcp Cd | |
| | TB | Experiment | TB | Experiment |
| $C_{11}$ | 168.52 | 179.09 | 134.37 | 129.23 |
| $C_{12}$ | 27.99 | 37.50 | 47.35 | 39.99 |
| $C_{13}$ | 28.92 | 55.40 | 33.66 | 40.95 |
| $C_{33}$ | 43.17 | 68.80 | 62.45 | 56.68 |
| $C_{44}$ | 24.04 | 45.95 | 22.24 | 24.20 |
| $C_{66}$ | 70.27 | 70.80 | 43.51 | 44.62 |
| $B$ | 40.74 | 66.09 | 52.81 | 52.51 |

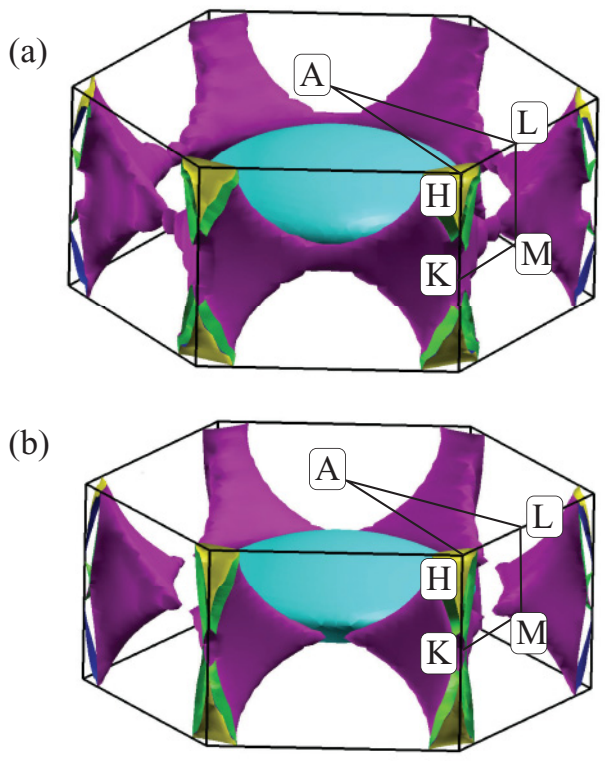


FIG. 4. (Color online) The tight-binding (a) and LAPW (b) calculated Fermi surfaces for hcp Zn. There are three bands, one forming pockets around the upper and lower parts of each corner (the $H$ point) (green/yellow); the second (purple/blue) filling the entire corner (the $K$-$H$ line) and maybe connecting the corners; and the third, in light blue, filling the zone center.

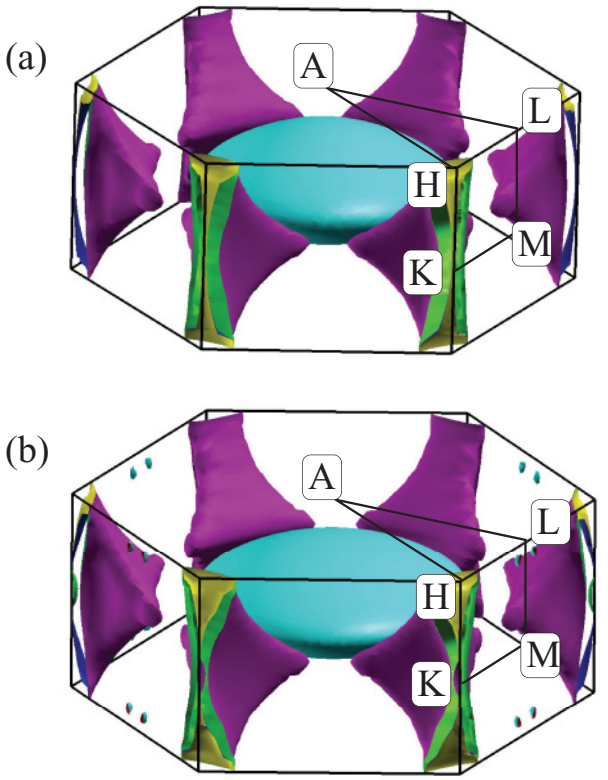


FIG. 5. (Color online) Same as Fig. 4, but for hcp Cd.

tight-binding molecular dynamics simulations at finite temperatures,[11]

$$\alpha = \frac{1}{3B}\left(\frac{\partial P}{\partial T}\right)_V, \tag{4}$$

where $B$ is the bulk modulus, $P$ is the temperature-dependent pressure, and $T$ is the temperature. We calculated $P$ using the usual virial definition[11,18] by adding up both the potential and kinetic contributions, and found a linear temperature dependence for both Zn and Cd, similar to that previously reported in several bcc transition metals.[18] Zn and Cd are both highly anisotropic, due to the unusually large $c/a$ ratios at their equilibrium hcp structures, so the experimentally measured linear thermal expansion coefficients vary significantly along the $a$ and $c$ axes. Our tight-binding calculated linear thermal expansion coefficients are in reasonable agreement with the average experimental values[57] (having the same order of magnitude), as shown in Table V.

### G. Vacancy formation energy

The computational efficiency of our tight-binding method enables us to examine large supercells, such as defect structures with minimal defect-defect interactions. Point defects such as monovacancies are intrinsic at high temperatures and have significant impact on a materials' thermal and mechanical properties. The thermal concentration of vacancies is usually associated with the vacancy formation energy $E_{vac}$, which can be obtained from our tight-binding calculations using[5]

$$E_{\rm vac}(V) = E_{\rm sc}(N-1,1;V) - (N-1)E_{\rm bulk}(V/N), \tag{5}$$

where $E_{sc}(M,Q;V)$ is the total energy of a supercell with volume $V$ containing $M$ atoms and $Q$ vacancies, and $E_{bulk}(V/N)$ is the total energy per atom for a bulk supercell of $N$ atoms with volume $V$. When calculating the total energy for the vacancy-contatining supercell, we ensure that the supercell is large enough to avoid the vacancy-vacancy interactions, and fully relax all the atoms using the conjugate gradient method while keeping the lattice symmetry. The calculated values are very sensitive to the supercell size and the number of $k$ points used in the tight-binding calculations. Using a supercell of $5 \times 5 \times 5$ which contains 249 metal atoms and one vacancy, we are able to obtain well-converged results of $E_{\rm vac}$ for both Zn and Cd when using 72 $k$ points in the tight-binding calculations, as shown in Table VI. In comparison to the experimental data measured from positron annihilation,[58] our

TABLE V. The tight-binding calculated linear coefficients of thermal expansion for hcp Cd and Zn both agree with experiment (Ref. 57).

| | Linear thermal expansion coefficient ($\times 10^{-5}$ K$^{-1}$) | |
|---|---|---|
| Element | TB | Experiment |
| Zn | 1.50 | 3.01 ($a$: 1.30, $c$: 6.43) |
| Cd | 2.43 | 3.13 ($a$: 1.98, $c$: 5.43) |

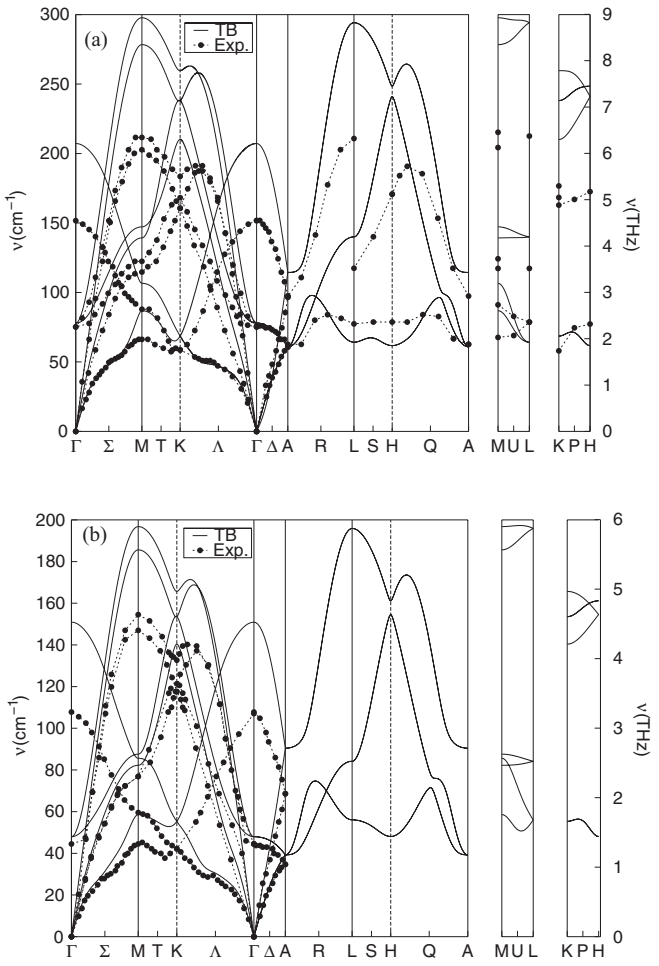


FIG. 6. The calculated phonon dispersion of hcp Zn (a) and Cd (b), in comparison to the inelastic neutron-scattering measurements (Ref. 51).

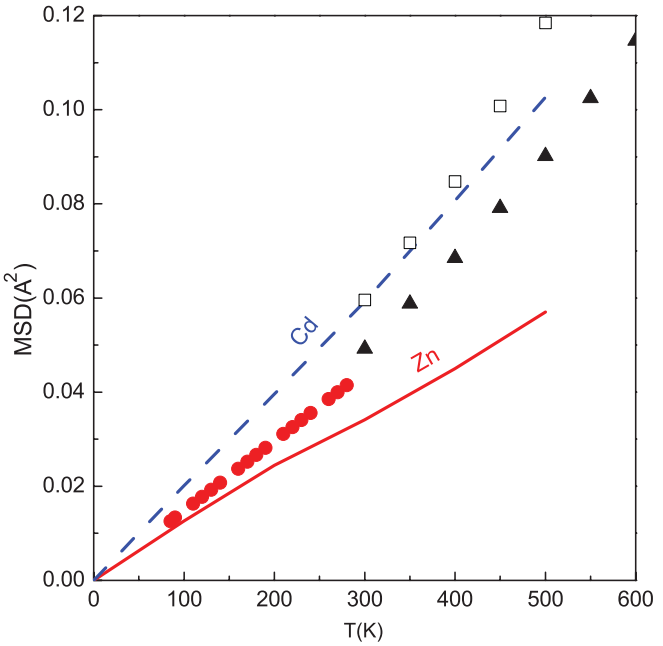


FIG. 7. (Color online) The temperature dependence of the atomic mean-square displacements for hcp Zn (solid line) and Cd (dashed line) calculated from tight-binding molecular dynamics simulations, in comparison to the experimental data derived from the Debye-Waller factor measurements (Zn, filled circles, Ref. 55; filled triangles, Ref. 56; Cd, open squares, Ref. 56).

tight-binding calculation overestimated the $E_{vac}$ for Cd and underestimated the value for Zn, by ∼0.3 eV. Both hcp Zn and Cd have very low vacancy formation energies, roughly one order of magnitude smaller than many of the transition metals we previously studied.[5,18] As shown in the band structure, the occupied *d* bands in Zn and Cd are located deep below the Fermi level, and most bands around the Fermi level have mixed *s* and *p* character. Thus Zn and Cd have electronic structures more similar to free-electron metals than transition metals. Aluminum, one of the free-electron metals which is not far from Zn in the periodic table, is reported to have a vacancy formation energy of 0.6 eV,[59] similar to the values of Zn and Cd.

## IV. CONCLUSIONS

In summary, we have developed NRL-TB Hamiltonians for Zn and Cd by fitting to first-principles LAPW band

TABLE VI. The tight-binding calculations underestimate the vacancy formation energy for hcp Zn and overestimate the value for hcp Cd, both by ∼0.30 eV, in comparison to the positron annihilation measurements (Ref. 58).

| | | | Vacancy formation energy (eV) | | | |
|---|---|---|---|---|---|---|
| | | | hcp Zn | | hcp Cd | |
| Supercell | No. of atoms | No. of *k* points | Unrelaxed | Relaxed | Unrelaxed | Relaxed |
| 4 × 4 × 4 | 128 | 32 | 0.428 | 0.218 | 0.951 | 0.617 |
| | | 48 | 0.475 | 0.272 | 0.971 | 0.643 |
| | | 72 | 0.494 | 0.295 | 1.032 | 0.708 |
| | | 108 | 0.491 | 0.291 | 1.033 | 0.709 |
| 5 × 5 × 5 | 250 | 32 | 0.447 | 0.214 | 1.100 | 0.740 |
| | | 48 | 0.480 | 0.248 | 1.086 | 0.732 |
| | | 72 | 0.454 | 0.222 | 1.049 | 0.689 |
| | | 108 | 0.487 | 0.258 | 1.049 | 0.690 |
| Experiment | | | 0.39 | | 0.52 | |

structures and total energies within the LDA, and applied the Hamiltonians to compute the ground-state behavior and phase stability, band structures, densities of states, elastic moduli, phonon frequencies, vacancy formation energies, mean-square displacements, and thermal expansion coefficients. We examined the tight-binding energies of 26 different crystal structures including many low-symmetry and defect systems, and find that hcp has the lowest energy for both Zn and Cd. The tight-binding calculated band structure, density of states, and Fermi surfaces agree well with first-principles LAPW results. The tight-binding bulk and elastic moduli of hcp Cd are in excellent agreement with experiment, and tight-binding calculations underestimate the bulk modulus and several elastic moduli for hcp Zn. The phonon spectra, calculated using the frozen phonon approximation, are in reasonable agreement with experiment. The calculated atomic mean-square displacements increase linearly with temperature, and hcp Cd has a larger MSD value over Zn at all temperatures, in good agreement with the Debye-Waller factor measurements. The calculated linear thermal expansion coefficients agree with experiment. The vacancy formation energies of Zn and Cd are roughly one order of magnitude lower than most transition metals, but close to the formation energy of aluminum.

## ACKNOWLEDGMENTS

Work at George Mason University was partially supported by Grants No. DGE0638680 from NIST and No. N00014-09-1-1025 from ONR. Work at the Naval Research Laboratory was sponsored by the US Office of Naval Research.

[1] J. C. Slater and G. F. Koster, Phys. Rev. **94**, 1498 (1954).
[2] D. A. Papaconstantopoulos and M. J. Mehl, J. Phys.: Condens. Matter **15**, 413 (2003).
[3] P. Hohenberg and W. Kohn, Phys. Rev. **136**, B864 (1964).
[4] W. Kohn and L. J. Sham, Phys. Rev. **140**, A1133 (1965).
[5] M. J. Mehl and D. A. Papaconstantopoulos, Phys. Rev. B **54**, 4519 (1996).
[6] R. E. Cohen, M. J. Mehl, and D. A. Papaconstantopoulos, Phys. Rev. B **50**, 14694 (1994).
[7] D. A. Papaconstantopoulos and M. J. Mehl, J. Phase Equilib. **18**, 593 (1997).
[8] S. H. Yang, M. J. Mehl, and D. A. Papaconstantopoulos, Phys. Rev. B **57**, 2013 (1998).
[9] F. Raouafi, C. Barreteau, M. C. Desjonqueres, and D. Spanjaard, Surf. Sci. **482**, 1413 (2001).
[10] E. Z. da Silva, A. J. R. da Silva, and A. Fazzio, Phys. Rev. Lett. **87**, 256102 (2001).
[11] F. Kirchhoff, M. J. Mehl, N. I. Papanicolaou, D. A. Papaconstantopoulos, and F. S. Khan, Phys. Rev. B **63**, 195101 (2001).
[12] Y. Mishin, M. J. Mehl, D. A. Papaconstantopoulos, A. F. Voter, and J. D. Kress, Phys. Rev. B **63**, 224106 (2001).
[13] M. J. Mehl, D. A. Papaconstantopoulos, I. I. Mazin, N. C. Bacalis, and W. E. Pickett, J. Appl. Phys. **89**, 6880 (2001).
[14] M. J. Mehl and D. A. Papaconstantopoulos, Europhys. Lett. **60**, 248 (2002).
[15] C. E. Lekka, M. J. Mehl, N. Bernstein, and D. A. Papaconstantopoulos, Phys. Rev. B **68**, 035422 (2003).
[16] D. Finkenstadt, N. Bernstein, J. L. Feldman, M. J. Mehl, and D. A. Papaconstantopoulos, Phys. Rev. B **74**, 184118 (2006).
[17] A. Shabaev and D. A. Papaconstantopoulos, Phys. Rev. B **79**, 064107 (2009).
[18] C. E. Lekka, N. Bernstein, D. A. Papaconstantopoulos, and M. J. Mehl, Mater. Sci. Eng., B **163**, 8 (2009).
[19] B. Akdim, D. A. Papaconstantopoulos, and M. J. Mehl, Philos. Mag. B **82**, 47 (2002).
[20] M. Lach-hab, B. Akdim, D. A. Papaconstantopoulos, M. J. Mehl, and N. Bernstein, J. Phys. Chem. Solids **65**, 1837 (2004).
[21] N. Bernstein, M. J. Mehl, and D. A. Papaconstantopoulos, Phys. Rev. B **66**, 075212 (2002).
[22] J. L. Feldman, N. Bernstein, D. A. Papaconstantopoulos, and M. J. Mehl, Phys. Rev. B **70**, 165201 (2004).
[23] J. L. Feldman, N. Bernstein, D. A. Papaconstantopoulos, and M. J. Mehl, J. Phys.: Condens. Matter **16**, S5165 (2004).
[24] D. A. Papaconstantopoulos and M. J. Mehl, Phys. Rev. B **64**, 172510 (2001).
[25] S. H. Yang, M. J. Mehl, D. A. Papaconstantopoulos, and M. B. Scott, J. Phys.: Condens. Matter **14**, 1895 (2002).
[26] C. E. Lekka, N. Bernstein, M. J. Mehl, and D. A. Papaconstantopoulos, Appl. Surf. Sci. **219**, 158 (2003).
[27] C. E. Lekka, D. A. Papaconstantopoulos, M. J. Mehl, D. Finkenstadt, and G. Evangelakis, J. Alloy. Compd. **483**, 627 (2009).
[28] T. A. Beu, J. Onoe, and K. Takeuchi, Eur. Phys. J. D **17**, 205 (2001).
[29] J. Cai, R. F. Bie, X. M. Tan, and C. Lu, Physica B **344**, 99 (2004).
[30] D. Finkenstadt, G. Pennington, and M. J. Mehl, Phys. Rev. B **76**, 121405 (2007).
[31] D. A. Papaconstantopoulos and W. E. Pickett, Phys. Rev. B **57**, 12751 (1998).
[32] I. I. Mazin, D. A. Papaconstantopoulos, and D. J. Singh, Phys. Rev. B **61**, 5223 (2000).
[33] D. A. Papaconstantopoulos, M. J. Mehl, and M. D. Johannes, Phys. Rev. B **82**, 054503 (2010).
[34] C. Kittel, *Introduction to Solid State Physics* (Wiley, New York, 1996).
[35] D. A. Papaconstantopoulos and M. J. Mehl, J. Phys.: Condens. Matter **15**, R413 (2003).
[36] O. K. Andersen, Phys. Rev. B **12**, 3060 (1975).
[37] S. H. Wei and H. Krakauer, Phys. Rev. Lett. **55**, 1200 (1985).
[38] M. P. Allen and D. J. Tildesley, *Computer Simulation of Liquids* (Clarendon, Oxford, 1989).
[39] D. D. Fitts, *Principles of Quantum Mechanics as Applied to Chemistry and Chemical Physics* (Cambridge University Press, Cambridge, UK, 1999).
[40] E. A. Carter, Science **321**, 800 (2008).
[41] X. Z. Wu, R. Wang, and S. F. Wang, Appl. Surf. Sci. **256**, 3409 (2010).
[42] T. Kenichi, Phys. Rev. B **60**, 6171 (1999).
[43] G. Steinle-Neumann, L. Stixrude, and R. E. Cohen, Phys. Rev. B **63**, 054103 (2001).

[44]M. Sigalas, D. A. Papaconstantopoulos, and N. C. Bacalis, Phys. Rev. B **45**, 5777 (1992).
[45]X. W. Sha and R. E. Cohen, Phys. Rev. B **81**, 094105 (2010).
[46]G. Simmons and H. Wang, *Single Crystal Elastic Constants and Calculated Aggregate Properties: A Handbook* (MIT Press, Cambridge, MA, 1971).
[47]U. Wedig, M. Jansen, B. Paulus, K. Rosciszewski, and P. Sony, Phys. Rev. B **75**, 205123 (2007).
[48]B. M. Klein and R. E. Cohen, Phys. Rev. B **45**, 12405 (1992).
[49]P. Giannozzi *et al.*, J. Phys.: Condens. Matter **21**, 395502 (2009).
[50]H. T. Stokes and L. L. Boyer (unpublished).
[51]B. Dorner, A. A. Chernyshov, V. V. Pushkarev, A. Y. Rumyantsev, and R. Pynn, J. Phys. F: Met. Phys. **11**, 365 (1981).
[52]S. Klotz and M. Braden, Phys. Rev. Lett. **85**, 3209 (2000).
[53]X. W. Sha and R. E. Cohen, Phys. Rev. B **74**, 214111 (2006).
[54]H. K. Mao *et al.*, Science **292**, 914 (2001).
[55]L. M. Peng, G. Ren, S. L. Dudarev, and M. J. Whelan, Acta Crystallogr., Sect. A: Found. Crystallogr. **52**, 456 (1996).
[56]P. D. Pathak and R. J. Desai, Phys. Status Solidi A **62**, 625 (1980).
[57]D. E. Gray, *American Institute of Physics Handbook* (McGraw-Hill, New York, 1972).
[58]B. T. A. McKee, W. Triftshäuser, and A. T. Stewart, Phys. Rev. Lett. **28**, 358 (1972).
[59]W. Triftshäuser, Phys. Rev. B **12**, 4634 (1975).